Open Access Library Journal
2026, Volume 13, e14974
ISSN Online: 2333-9721
ISSN Print: 2333-9705

Neural Network Approximation Based on ANFIS and Geographic Information System Mapping for Reliable Evapotranspiration Prediction in Khenchela, Algeria

Assia Meziani[1*], Nabil Mega[1], Abdelmonen Miloudi[1], António Canatário Duarte[2,3,4], Abderahamane Khechekhouche[1]

[1]New Technology and Local Development Laboratory, Department of Hydraulic and Civil Engineering, Faculty of Technology, University of El-Oued, El-Oued, Algeria
[2]School of Agriculture, Polytechnic University of Castelo Branco, Castelo Branco, Portugal
[3]Research Center for Natural Resources, Environment and Society, IPCB, Castelo Branco, Portugal
[4]Research Center of Geobiosciences, Geoengineering, and Geotechnologies, University of Beira Interior, Covilhã, Portugal
Email: *assia-meziani@univ-eloued.dz

How to cite this paper: Meziani, A., Mega, N., Miloudi, A., Duarte, A.C. and Khechekhouche, A. (2026) Neural Network Approximation Based on ANFIS and Geographic Information System Mapping for Reliable Evapotranspiration Prediction in Khenchela, Algeria. *Open Access Library Journal*, **13**: e14974.
https://doi.org/10.4236/oalib.1114974

Received: February 2, 2026
Accepted: March 2, 2026
Published: March 5, 2026

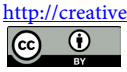

Abstract

Accurate estimation of reference evapotranspiration (ET_0) is critical for sustainable water resource management, irrigation scheduling, and climate adaptation in heterogeneous semi-arid regions. This study presents a streamlined neural network (NN) approximation inspired by the Adaptive Neuro-Fuzzy Inference System (ANFIS) for predicting daily ET_0 in Khenchela province, northeastern Algeria. Utilizing meteorological and soil data from 2000 to 2024 at 16 representative stations (Babar (1), Babar (2), Babar (3), Baghai, Bouhmama, Chechar, Djellal, El Hamma, Kais, Khenchela, Khirane, M'sara, Remila, Tamza, Taouzient, and Zaoui), sourced from the Open-Meteo Historical Weather API, the model employs inputs including air temperature, relative humidity, precipitation, wind speed, sunshine duration, terrestrial radiation, soil temperature, and soil moisture. The NN was trained to closely approximate the FAO-56 Penman-Monteith reference ET_0 values computed directly by the API. Performance evaluation yielded strong agreement across stations: $R^2 > 0.96$, RMSE 0.22 - 0.46 mm/day, NSE > 0.95, RSR < 0.13, and Willmott's index 0.88 - 0.93, with peak accuracy ($R^2 > 0.99$, RMSE < 0.24 mm/day) at high-elevation sites. Spatial patterns, mapped via GIS-based inverse distance weighting interpolation, revealed pronounced topographic and aridity-driven variability, confirmed by Emberger and De Martonne indices. This computationally efficient NN offers a scalable surrogate for FAO-56 calculations in data-limited, heter-

ogeneous environments, supporting precision irrigation, drought monitoring, and adaptive strategies in semi-arid North Africa and Mediterranean regions.

Subject Areas

Agricultural Engineering

Keywords

Evapotranspiration, Neural Network, ANFIS, Modeling, Khenchela, Algeria

1. Introduction

Reference evapotranspiration (ET_0) is a multifaceted hydrological variable influenced by numerous climatic factors that govern water and energy balances [1]. It plays a pivotal role in hydro-climatological processes and directly impacts agricultural production [2]. The importance of evapotranspiration extends across disciplines such as ecology, hydrology, and meteorology [3], serving as a key component in understanding the hydrological cycle and supporting applications including irrigation requirement estimation, irrigation scheduling, water resource management, and assessment of climate change effects [4]-[6]. Various methods exist to measure or estimate evapotranspiration and its components across scales—from plant-level to atmospheric boundary-layer analyses reflecting its multidisciplinary nature. These include direct techniques (e.g., lysimeters) and indirect approaches relying on meteorological data [7]. Direct measurements provide high accuracy but are costly, time-intensive, and limited in spatial coverage for regional applications [8]. Indirect empirical methods based on comprehensive climate data offer reliable, cost-effective alternatives for long-term and large-scale estimation [1] [6].

The FAO-56 Penman-Monteith (FAO-56 PM) method stands as the established benchmark for estimating reference ET_0 across diverse climates, widely validated and recommended by international bodies [9] [10]. As a physically based approach, it requires extensive climatic inputs (e.g., temperature, humidity, wind speed, radiation), which can pose challenges in data-scarce or heterogeneous environments [11]. In such contexts, machine learning (ML) models—particularly the Adaptive Neuro-Fuzzy Inference System (ANFIS)—provide robust alternatives by effectively capturing nonlinear relationships among variables [12].

This study introduces a novel streamlined neural network (NN) approximation inspired by ANFIS to estimate daily reference ET_0 in the heterogeneous semi-arid region of Khenchela province, northeastern Algeria. The target variable for model training, validation, and evaluation is the reference ET_0 computed using the FAO-56 Penman-Monteith method, as directly provided by the Open-Meteo Historical Weather API (variable: et_0 (fao_evapotranspiration)). This value is derived internally from reanalysis-based meteorological inputs (temperature, relative humid-

ity, wind speed, solar/terrestrial radiation) following the standard FAO-56 equations, assuming unlimited soil water availability for a hypothetical well-watered grass reference crop. Unlike conventional ANFIS architectures that incorporate explicit fuzzy rule layers, the proposed NN employs a tanh-activated hidden layer to implicitly approximate fuzzy-like relationships, reducing computational complexity while maintaining accuracy. This design enhances suitability for data-limited regions and builds upon prior ML-based ET_0 studies [2] [13] by offering improved scalability. The methodology is intended to be generalizable to other semi-arid areas, addressing gaps in localized, efficient ET_0 modeling. The NN is evaluated against the FAO-56 PM values from Open-Meteo to assess its effectiveness as a computationally efficient surrogate in heterogeneous terrains.

2. Materials and Methods

2.1. Study Area

Khenchela, located in northeastern Algeria (**Figure 1**), exhibits various topographies, ranging from semi-arid flats to mountain ranges, which leads to climate variability. This region is located in the Aures Mountains (Batna), resulting in a large variation in elevation, which leads to the formation of unique microclimates. Sixteen meteorological stations are evenly distributed throughout the province, covering different climatic conditions and altitudes: Babar (1), Babar (2), Babar (3), Baghai, Bouhmama, Chechar, Djellal, El Hamma, Kais, Khenchela, Khirane, M'sara, Remila, Tamza, Taouzient, and Zaoui. Stations such as Khenchela and Kais, located in either urbanized or lowland areas, experience moderate temperatures for various reasons, whereas stations at higher elevations, such as Tamza and Bouhmama, experience cooler temperatures and increased precipitation owing to their mountainous climate. The other three stations in the south, Babar (1, 2, and 3) experienced drier and warmer climates. This diversity makes Khenchela ideal for testing ET models applicable to semi-arid regions globally.

Climatic data (2000-2024) were sourced from the Open-Meteo Historical Weather API (2024), including air temperature (˚C), relative humidity (%), precipitation (mm), wind speed (km/h), soil temperature (˚C), soil moisture (m^3/m^3), sunshine duration (s), and terrestrial radiation (W/m^2). Data preprocessing involved normalizing inputs to a [0, 1] range using min-max scaling and handling missing values through linear interpolation, ensuring data quality. Therefore, we analyzed 16 locations as semi-arid, arid, and hyper-arid zones based on precipitation (P), and Emberger rainfall quotient (Q_2) which uses the maximum (M) and minimum (m) mean temperatures of the hottest and coldest months. The findings revealed a significant correlation between precipitation and aridity levels, with semi-arid regions receiving an average of 495.3 mm of rainfall, compared to 284.1 mm in arid zones and 95.43 mm in hyper-arid areas (**Table 1**).

Precipitation (P), Minimum mean temperature of the coldest month in ˚C (m), Maximum mean temperature of the hottest month in ˚C (M), and Emberger rainfall quotient (Q_2).

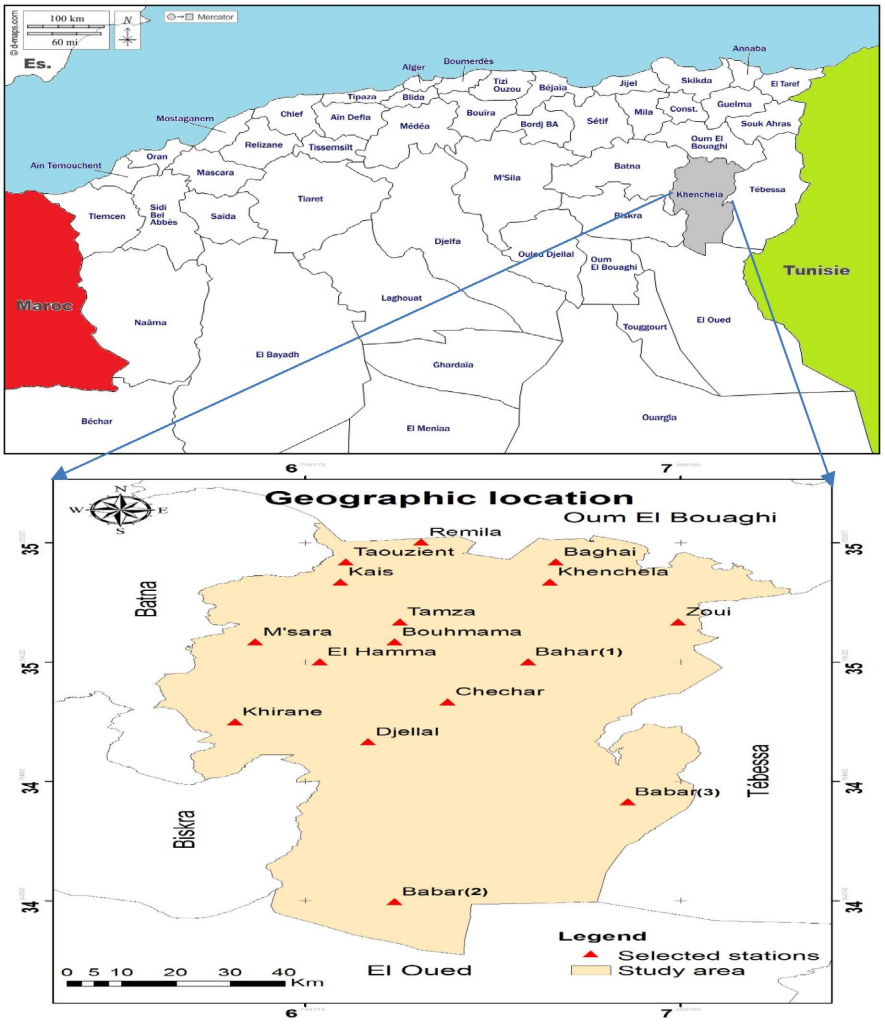

Figure 1. Localization of 16 stations in Khenchela region (Algeria) [14].

The De Martonne aridity index (M) plays a crucial role in the aridity classification. This study found that semi-arid regions experienced milder climatic conditions (M ≈ 32.6), whereas arid and hyper-arid regions exceeded 34, reaching up to 40.92 in extreme cases (**Table 1**). However, the mean minimum temperature of the coldest month varied across the regions, ranging from negative to approximately 5˚C. The Emberger rainfall quotient, a climatic indicator, shows that higher precipitation levels directly influence the water availability. Semi-arid locations exhibit superior hydrological conditions, whereas hyper-arid zones are characterized by extreme dryness and minimal runoff. These findings underscore the need for targeted water conservation strategies, in which climate adaptation strategies should prioritize sustainable water management, afforestation efforts, and resilient agricultural practices in semi-arid regions, and advanced irrigation and water conservation techniques should be implemented in arid and hyper-arid areas.

Table 1. Aridity indices of the sixteen stations located in Khenchela region.

Stations	P (mm)	m	M	Q_2	Aridity
Babar (1)	472.93	0.927	33.963	49.289	Semi-arid
Babar (2)	95.432	4.793	40.923	8.928	Hyper-arid
Babar (3)	119.160	5.038	37.938	12.299	Arid
Chechar	302.064	1.080	32.796	32.848	Arid
Djellal	252.408	3.298	34.824	27.413	Arid
Khirane	157.172	2.773	35.839	16.261	Arid
M'sara	506.048	-0.052	31.833	54.936	Semi-Arid
El-Hamma	388.700	0.607	34.297	39.722	Arid
Bouhmama	390.812	0.480	34.114	40.025	Arid
Tamza	446.424	-0.088	32.568	47.263	Semi-arid
Taouzient	557.764	3.324	33.870	62.621	Semi-arid
Remila	307.336	1.407	35.328	31.095	Arid
Kais	376.580	1.874	34.800	39.257	Arid
Zaoui	359.728	0.953	33.224	38.425	Arid
Baghai	329.364	1.718	35.043	33.919	Arid
Khenchela	360.452	0.809	33.933	37.477	Arid

2.2. Evapotranspiration Prediction Methods (FAO-56 and Neural Network Approximation Inspired by ANFIS Model)

The accuracy and reliability of evapotranspiration calculations for several land-use types have been considerably improved by FAO-56 [15]. FAO-56 has been validated globally against lysimeter data by several international organizations, including the International Commission on Irrigation and Drainage, FAO, and the American Society of Civil Engineers, confirming that these methods can be used to compute potential evapotranspiration using climate data [16] [17]. The FAO-56 Penman-Monteith equation is expressed as follows:

$$ET_0 = \frac{0.408\Delta\left(R_n - G\right) + \gamma \dfrac{900}{T+273} u_2 \left(e_s - e_a\right)}{\Delta + \gamma\left(1 + 0.34u_2\right)} \quad (1)$$

where:

ET_0 = Reference Evapotranspiration (mm day $^{-1}$); R_n = Net radiation at crop surface (MJm^{-2} d $^{-1}$); G = Soil heat flux density (MJm^{-2} d $^{-1}$); T = Mean daily air temperature at 2 m height $\left(^{\circ}C\right)$; u_2 = Wind speed at 2 m height $\left(ms^{-1}\right)$; e_s = Saturation vapor pressure $\left(kPa\right)$; e_a = Actual vapor pressure $\left(kPa\right)$; $e_s - e_a$ = Vapor pressure deficit $\left(kPa\right)$; Δ = Slope of saturation vapor pressure curve $\left(kPa\,^{\circ}C^{-1}\right)$

The reference evapotranspiration (ET_0) used as the "observed" target for training, validation, and testing the neural network was the FAO-56 Penman-Mon-

teith ET_0 value directly retrieved from the Open-Meteo Historical Weather API (variable: et0_fao_evapotranspiration, in mm/day after aggregation/summing from hourly values) [18]. This value is computed internally by Open-Meteo using the standard FAO-56 equations applied to reanalysis-derived meteorological inputs (temperature, relative humidity, wind speed, solar/terrestrial radiation). No in-situ lysimeter measurements or independent ground-based ET_0 estimates were used; thus, the NN serves as a surrogate model to approximate the FAO-56 benchmark rather than an alternative that outperforms it on independent observations.

2.3. Neural Network Approximation Inspired by ANFIS

The ANFIS model, recognized for its acceptable performance in hydrological applications such as estimating solar radiation and pan evaporation, is considered a valuable approach for dealing with complex, nonlinear relationships that comprise the processes of evapotranspiration [2]. ANFIS uses this adaptive mechanism to model complex nonlinear relationships between variables, and is therefore particularly appropriate for the uncertain and imprecise tasks inherent in hydrological modeling [15]. Moreover, optimization algorithms can be applied to estimate the parameters of ANFIS more effectively to decrease the error in the prediction of the reference evapotranspiration. The architecture serves as a simplified approximation of the ANFIS model (**Figure 2**) because it does not have explicit fuzzy rule layers, normalization, or defuzzification components. The neural network implicitly learns fuzzy-like relationships based on the tanh activation and dense layers. Python code creates a neural network with the following layout:

- **Input layer:** Inputs: Twelve features based on the selected columns (e.g., temperature and humidity) after normalization. • Shape: (12). There are 12 input features.
- **Hidden layer (membership function approximation)**: A dense layer with five hidden neurons. Activation: tanh, which approximates the role of membership functions in ANFIS. • Purpose: Hidden layers attempt to imitate fuzzification by converting input features into nonlinear representations.
- **Output layer:** dense layer with one neuron. • Activation: Linear (default, regression tasks). • Purpose: This architecture provides the final predicted evapotranspiration value.
- **Training-validation and test:** • Optimizer: Adam • Loss function: mean squared error (MSE). • Metrics: Mean absolute error (MAE). • Epoch count: 50; batch size: 32.

The first step of the script was to import the relevant libraries to perform the task. The following functionalities were imported: Numpy and Pandas handled the numerical calculations and data manipulation. Modules from the scikit-learn package were used to assist with pre-processing, data splitting, and evaluation metrics. The TensorFlow and Keras modules were used to train the neural net-

work model. The developed Python script executes a model based on a neural network inspired by ANFIS-structured artificial neural networks (ANNs) to estimate the reference ET from meteorological and soil data. The process consisted of data preprocessing, model training, evaluation, and post-processing of the results (Figure 3).

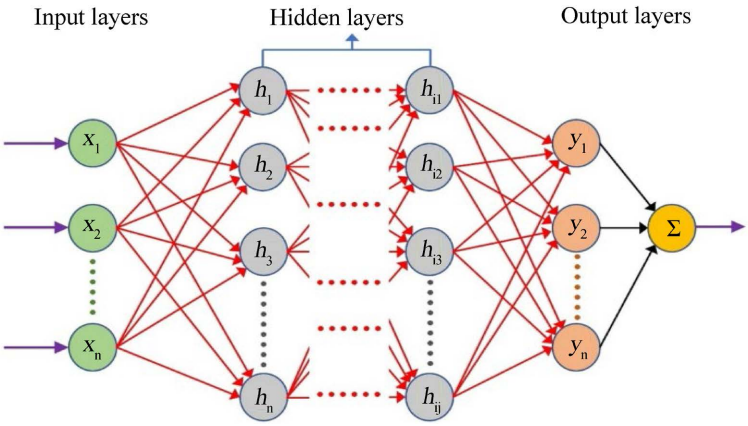

Figure 2. Architecture of NN approximation based on ANFIS.

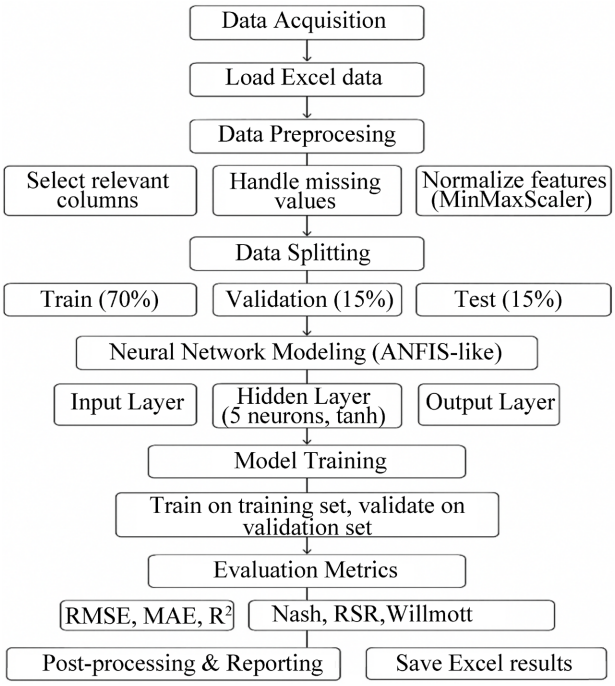

Figure 3. Neural network modeling and evaluation workflow.

To supplement the conventional metrics, three distinct hydrological performance metrics were created: Nash-Sutcliffe Efficiency (Nash), which measures the predictive capacity in relation to the observed data variance. The root sum ratio (RSR) was calculated as the ratio of the RMSE to the standard deviation of observed data. Willmott's index captures the concordance between the predicted and

observed values with deviations from the mean. The presence of these functions implies that the model was judged based on domain-specific and conventional hydrological evaluation metrics (**Figure 3**). GIS mapping used inverse distance weighting (IDW) interpolation to visualize spatial ET patterns, leveraging station data to estimate regional trends.

2.4. Data Splitting

The dataset consists of daily records from 2000 to 2024 across the 16 stations [18]. To respect the temporal nature of the data and prevent information leakage from future observations into model training, a chronological blocking (time-based sequential split) was applied rather than random shuffling. Specifically :

- Training set: 2000-2017 (~70% of the period, earliest years)
- Validation set: 2018-2021 (~15%, intermediate period for hyperparameter tuning and early stopping)
- Test set: 2022-2024 (~15%, most recent years for final out-of-sample evaluation)

Missing data (<5% of records) were imputed using linear interpolation. Sensitivity analysis showed model stability across ±10% variations in input parameters.

The input features include calendar info (year, month, day), air temperature at 2 m (˚C), relative humidity (%), dew point (˚C), total daily precipitation (mm), surface pressure (hPa), vapour pressure deficit (kPa), wind speed at 10 m height (given in km/h), soil temperature and moisture in the top 0 - 7 cm, daily sunshine duration (in seconds), and terrestrial radiation (in W/m^2). All these values appear to be daily aggregates.

3. Results and Discussion

The neural network approximation inspired by the ANFIS model displayed excellent predictive accuracy for estimating ET in systems with various climatic conditions across the 16 stations (**Table 2**, **Table 3**, and **Table 4**), with small variability from local climatological conditions. Three stations (Babar 2, Babar 3, and Khirane) exhibited strong estimation accuracies, as indicated by their RMSE (<0.32), R^2 (>0.99), and RSR (<0.11) values. Willmott's index at each station was between 0.92 and 0.93, indicating an excellent agreement between the observed and predicted ET. These results demonstrate the strength of the model's ability to estimate the ET nonlinearity in these systems. Eight stations (Baghai, Bouhmama, Chechar, Djellal, Khenchela, Remila, Tamza, and Taouzient) performed moderately well, with RMSE values ranging from 0.24 - 0.29 and R^2 (>0.98). These results resulted in RSR values of approximately 0.12 - 0.15, with Willmott's index ranging from 0.88 to 0.91, thereby confirming our predictions. At some of these stations, the slightly higher RMSE may have been influenced by moderately greater climatic variability or localized data errors. Three stations (Babar 1, El Hamma, and Kais) exhibited slightly higher RMSE values, up to 0.32, with strong R^2 values (>0.97). Willmott's index ranged from 0.84 to 0.89, indicating moderate to good agree-

ment between the model outputs and the observed ET estimations. The Zaoui station showed reliable performance, with RMSE, MAE, and R^2 (>0.94) still within the acceptable range. The reliability of the model was also demonstrated, where ANFIS estimation with local climatic variation closely predicted ET using the FAO Penman-Monteith equation. The neural network approximation accurately predicted ET at all stations. The ability of the model to account for complex nonlinear relationships was evident at stations with lower RMSE and higher R^2 values (Babar 2, Babar 3, and Khirane). The RMSE variability across stations appears to be linked to localized factors or data variability within the same station. All stations exhibited low RSR values and high Willmott's index values, confirming the power and reliability of the model for estimating ET under different meteorological conditions.

The maps (**Figure 4(a)-(e)**) show the spatial patterns of the predicted mean annual ET in the Khenchela region of eastern Algeria. Maps were obtained by interpolating the station observations (**Figure 1**). From 2000 to 2005, ET demonstrated a downward trend, with a cumulative loss of ~8 - 15% across stations, largely in the northern and central areas. The regional mean ET fell from 143.3 mm yr^{-1} (2000-2001) to 130.8 mm yr^{-1} (2003-2004), with a small rebound to 135.8 mm yr^{-1} in 2005. This is represented by contour contraction: high values in red (>150 mm yr^{-1}) shrink in areas around Khirane and Tebessa, and low values in blue expand to the north of the study area. Linear regression showed statistically significant negative trends at the northern/central stations (**Table 2**), with slopes of −3.0 mm yr^{-1} $decade^{-1}$ at Kais and Khirane ($p < 0.05$, $R^2 = 0.66$). These trends may reflect interannual variability in precipitation or the greenness of vegetation, which is likely linked to episodic drought events (e.g., reduced winter precipitation). The southern stations had weaker, non-significant trends (slopes of −1.7 to −2.1 mm yr^{-1} $decade^{-1}$; $p > 0.10$), possibly indicating more stable control against short-term fluctuations due to more dominant evaporative control. The increase in 2005 (~5 - 10 mm yr^{-1} increase) coincided with the southern contour expansion, possibly indicating a temporary wet anomaly in the region. These patterns correlate with elevation and soil moisture, with semi-arid regions showing higher ET than arid/hyper-arid zones.

Table 2. Performance metrics for the 16 stations (Training data from 2000 to 2017).

Metric	1	2	3	4	5	6	7	8	9	10	11	12	13	14	15	16
RMSE	0.509	0.306	0.265	0.285	0.296	0.256	0.245	0.301	0.318	0.273	0.235	0.294	0.279	0.292	0.291	0.265
MAE	0.343	0.218	0.189	0.216	0.227	0.194	0.185	0.227	0.241	0.206	0.176	0.223	0.213	0.223	0.220	0.203
R^2	0.944	0.990	0.991	0.982	0.979	0.985	0.987	0.979	0.977	0.984	0.990	0.978	0.982	0.978	0.981	0.984
NASH	0.944	0.990	0.991	0.982	0.979	0.985	0.987	0.979	0.977	0.984	0.990	0.978	0.982	0.978	0.981	0.984
RSR	0.237	0.099	0.096	0.133	0.144	0.123	0.114	0.146	0.151	0.127	0.099	0.150	0.134	0.149	0.139	0.125
Wi	0.844	0.925	0.927	0.895	0.887	0.903	0.910	0.887	0.882	0.899	0.922	0.884	0.894	0.884	0.891	0.900

Table 3. Performance metrics for the 16 stations (Validation data from 2018 to 2021).

Metric	1	2	3	4	5	6	7	8	9	10	11	12	13	14	15	16
RMSE	0.476	0.317	0.249	0.271	0.285	0.249	0.241	0.289	0.307	0.266	0.231	0.291	0.271	0.284	0.274	0.259
MAE	0.326	0.226	0.183	0.207	0.217	0.189	0.185	0.216	0.233	0.202	0.171	0.216	0.205	0.215	0.209	0.195
R^2	0.947	0.989	0.991	0.983	0.979	0.984	0.986	0.979	0.977	0.983	0.990	0.976	0.982	0.977	0.981	0.984
NASH	0.947	0.989	0.991	0.983	0.979	0.984	0.986	0.979	0.977	0.983	0.990	0.976	0.982	0.977	0.981	0.984
RSR	0.231	0.106	0.093	0.132	0.144	0.125	0.116	0.145	0.151	0.130	0.101	0.154	0.135	0.151	0.136	0.127
Wi	0.845	0.919	0.926	0.895	0.887	0.902	0.906	0.888	0.882	0.897	0.921	0.882	0.893	0.882	0.891	0.900

Table 4. Performance metrics for the 16 stations (Testing data from 2022 to 2024).

Metric	1	2	3	4	5	6	7	8	9	10	11	12	13	14	15	16
RMSE	0.490	0.300	0.255	0.259	0.285	0.250	0.236	0.286	0.292	0.258	0.239	0.282	0.265	0.280	0.264	0.254
MAE	0.321	0.217	0.183	0.201	0.216	0.187	0.181	0.217	0.225	0.197	0.174	0.213	0.207	0.216	0.205	0.191
R^2	0.946	0.990	0.991	0.985	0.980	0.985	0.988	0.980	0.980	0.985	0.990	0.979	0.983	0.979	0.983	0.985
NASH	0.946	0.990	0.991	0.985	0.980	0.985	0.988	0.980	0.980	0.985	0.990	0.979	0.983	0.979	0.983	0.985
RSR	0.232	0.099	0.094	0.123	0.140	0.122	0.111	0.140	0.141	0.122	0.101	0.146	0.129	0.145	0.129	0.121
Wi	0.850	0.923	0.928	0.900	0.890	0.905	0.911	0.890	0.888	0.901	0.922	0.886	0.895	0.885	0.896	0.903

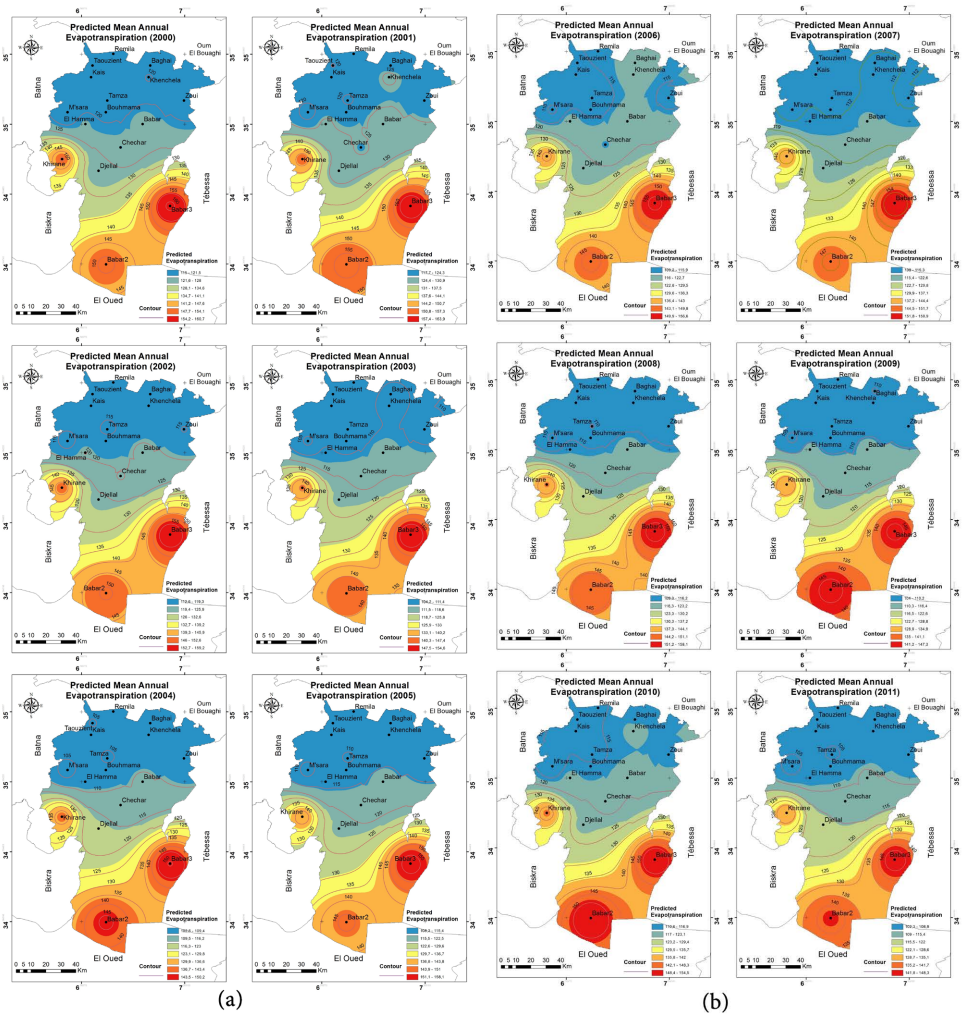

(a) (b)

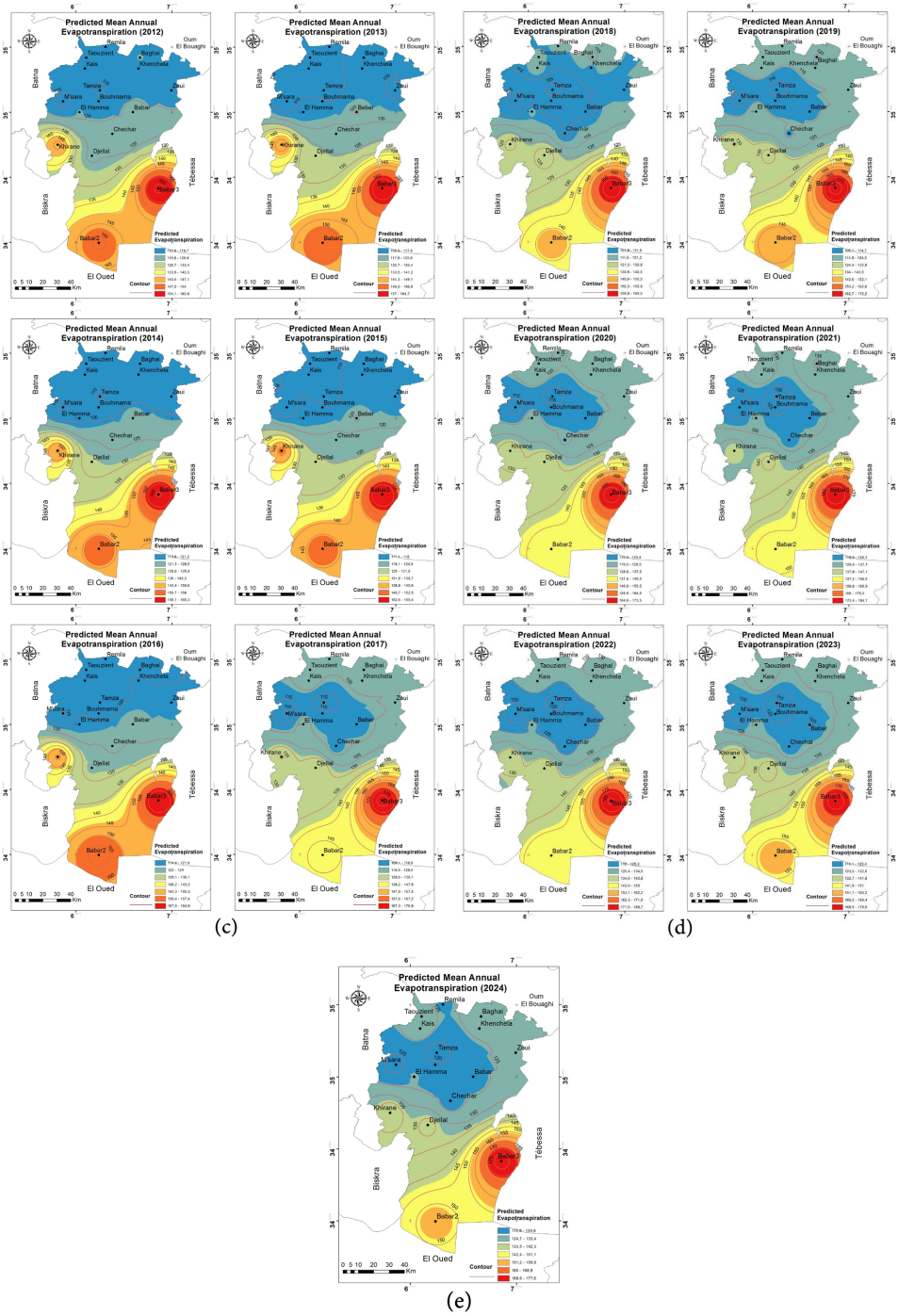

Figure 4. (a) Neural network approximation inspired by ANFIS-based mapping of mean annual evapotranspiration for 2000-2005; (b) Neural network approximation inspired by ANFIS-based mapping of mean annual evapotranspiration for 2006-2011; (c) Neural network approximation inspired by ANFIS-based mapping of mean annual evapotranspiration for 2012-2017; (d) Neural network approximation inspired by ANFIS-based mapping of mean annual evapotranspiration for 2018-2023; (e) Neural network approximation inspired by ANFIS-based mapping of mean annual evapotranspiration for 2024.

Sixteen training stations were used: Babar 1 (1), Babar 2 (2), Babar 3 (3), Baghai

(4), Bouhmama (5), Chechar (6), Djellal (7), El Hamma (8), Kais (9), Khenchela (10), Khirane (11), M'sara (12), Remila (13), Tamza (14), Taouzient (15), and Zaoui (16).

4. Conclusion

This study effectively established the usefulness of a neural network inspired by the adaptive neuro-fuzzy inference system (ANFIS) integrated with a Geographic Information System (GIS) to predict and spatially map ET in the heterogeneous climatic context of the Khenchela region in Algeria. Using historical climate data from 16 sites from 2000 to 2024, the neural network model performed well ($R^2 > 0.94$, RMSE ranged from 0.23 to 0.50). Specific sites (Babar (2), Babar (3), and Khirane) were accurate ($R^2 > 0.99$, RMSE < 0.27), demonstrating the ability of the approximation method to capture localized climatic conditions. In comparison, station Babar (1) had higher predictive errors, signaling ET on spacing, and topographic, arid, and other environmental variations. The neural network model also demonstrated strong generalizability with low root sum errors (RSR < 0.15), close to one Nash-Sutcliffe efficiency (NSE), and Willmott's index between 0.84 and 0.92, highlighting its reliability over other methods, such as the FAO-56 Penman-Monteith ET_0 values from Open-Meteo ($R^2 > 0.94$, RMSE 0.23 - 0.50 mm/day), highlighting its reliability as an efficient approximation in areas with heterogeneous climates or limited computational resources. Spatial mapping using GIS showed that ET spatial variability was related to elevation, rainfall, and soil characteristics, with semi-arid regions showing higher ET values than arid and hyper-arid regions. These results demonstrate that neural network approximation provides a good degree of flexibility.

Acknowledgements

I sincerely thank Nabil Mega for his excellent work in preparing the GIS visualizations and spatial interpolation maps (**Figure 1** and **Figure 4(a)-(e)**). I am grateful to Abdelmonen Miloudi for carrying out the formal analysis, model validation, and compilation of the performance metrics presented in **Tables 2-4**. I also express my deep appreciation to António Canatário Duarte and Abderahamane Khechekhouche for their thorough critical reviews, valuable suggestions, and insightful contributions to strengthening the manuscript.

Conflicts of Interest

The authors declare no conflicts of interest.

References

[1] Ayaz, A., Rajesh, M., Singh, S.K. and Rehana, S. (2021) Estimation of Reference Evapotranspiration Using Machine Learning Models with Limited Data. *AIMS Geosciences*, **7**, 268-290. https://doi.org/10.3934/geosci.2021016

[2] Aghelpour, P., Varshavian, V. and Hamedi, Z. (2022) Comparing the Models

SARIMA, ANFIS and ANFIS-DE in Forecasting Monthly Evapotranspiration Rates under Heterogeneous Climatic Conditions. *Scientific Reports*, **12**, Article No. 17363.

[3] Wilson, K.B., Hanson, P.J., Mulholland, P.J., Baldocchi, D.D. and Wullschleger, S.D. (2001) A Comparison of Methods for Determining Forest Evapotranspiration and Its Components: Sap-Flow, Soil Water Budget, Eddy Covariance and Catchment Water Balance. *Agricultural and Forest Meteorology*, **106**, 153-168. https://doi.org/10.1016/s0168-1923(00)00199-4

[4] Kumar, J., Suresh, R. and Kumar, D. (2017) Comparison of Reference Evapotranspiration Determining Methods Using Climatic Data of Pusa. *International Journal of Current Microbiology and Applied Sciences*, **6**, 627-637. https://doi.org/10.20546/ijcmas.2017.610.077

[5] Lu, Y., Wen, M., Li, P., Liang, J., Wei, H. and Li, M. (2023) An Improved Craig-Gordon Isotopic Model: Accounting for Transpiration Effects on the Isotopic Composition of Residual Water during Evapotranspiration. *Agronomy*, **13**, Article 1531. https://doi.org/10.3390/agronomy13061531

[6] Moorhead, J.E., Gowda, P.H., Marek, G.W., Porter, D. and Marek, T. (2016) Spatial Uniformity in Sensitivity Coefficient of Reference ET in the Texas High Plains. *Applied Engineering in Agriculture*, **32**, 263-269.

[7] Tilahun, K. (2006) Analysis of Rainfall Climate and Evapo-Transpiration in Arid and Semi-Arid Regions of Ethiopia Using Data over the Last Half a Century. *Journal of Arid Environments*, **64**, 474-487. https://doi.org/10.1016/j.jaridenv.2005.06.013

[8] Ramachandra, J.T., Veerappa, S.R.N. and Udupi, D.A. (2021) Assessment of Spatio-temporal Variability and Trend Analysis of Reference Crop Evapotranspiration for the Southern Region of Peninsular India. *Environmental Science and Pollution Research*, **29**, 41953-41970. https://doi.org/10.1007/s11356-021-15958-0

[9] Bhartiya, K.M. and Ghare, A.D. (2015) Reference Evapotranspiration in Agro-Climatic Regions of India. *Proceedings of the Institution of Civil Engineers—Water Management*, **168**, 37-44. https://doi.org/10.1680/wama.13.00124

[10] Ferreira, L.B., Duarte, A.B., Cunha, F.F.D. and Fernandes Filho, E.I. (2019) Multivariate Adaptive Regression Splines (MARS) Applied to Daily Reference Evapotranspiration Modeling with Limited Weather Data. *Acta Scientiarum. Agronomy*, **41**, e39880. https://doi.org/10.4025/actasciagron.v41i1.39880

[11] Zakhrouf, M., Bouchelkia, H. and Stamboul, M. (2019) Neuro-Fuzzy Systems to Estimate Reference Evapotranspiration. *Water SA*, **45**, 133-140. https://doi.org/10.4314/wsa.v45i2.10

[12] Chia, M.Y., Huang, Y.F. and Koo, C.H. (2020) Reference Evapotranspiration Estimation Using Adaptive Neuro-Fuzzy Inference System with Limited Meteorological Data. *IOP Conference Series: Earth and Environmental Science*, **612**, Article ID: 012017. https://doi.org/10.1088/1755-1315/612/1/012017

[13] Aly, M.S., Darwish, S.M. and Aly, A.A. (2023) High Performance Machine Learning Approach for Reference Evapotranspiration Estimation. *Stochastic Environmental Research and Risk Assessment*, **38**, 689-713. https://doi.org/10.1007/s00477-023-02594-y

[14] D-Maps (2025) Free Maps of Countries, Regions, and Continents. https://d-maps.com/

[15] Allen, R.G., Pereira, L.S., Raes, D. and Smith, M. (1998) Crop Evapotranspiration: Guidelines for Computing Crop Water Requirements, FAO Irrigation and Drainage Paper 56. Food and Agriculture Organization of the United Nations.

[16] Sun, S., Bi, Z., Xiao, J., Liu, Y., Sun, G., Ju, W., *et al.* (2023) A Global 5 Km Monthly Potential Evapotranspiration Dataset (1982-2015) Estimated by the Shuttleworth-Wallace Model. *Earth System Science Data*, **15**, 4849-4876. https://doi.org/10.5194/essd-15-4849-2023

[17] Akiner, M.E. and Ghasri, M. (2024) Comparative Assessment of Deep Belief Network and Hybrid Adaptive Neuro-Fuzzy Inference System Model Based on a Meta-Heuristic Optimization Algorithm for Precise Predictions of the Potential Evapotranspiration. *Environmental Science and Pollution Research*, **31**, 42719-42749. https://doi.org/10.1007/s11356-024-33987-3

[18] Open-Meteo (2024) Historical Weather API. https://open-meteo.com